Fracture Mechanics of Concrete Structures, de Borst et al (eds) © 2001 Swets & Zeitlinger, Lisse, ISBN 90 2651 825 0

HPFRC pre-stressed thin-web elements: some results on shear resistance

Marco di Prisco & Liberato Ferrara
Department of Structural Engineering, Politecnico di Milano, Italy

ABSTRACT: Steel fibres improve the mechanical characteristics of high-strength concrete: their use in pre-cast thin-web elements can be regarded interesting in terms of simplicity and economy only if alternative to traditional transversal reinforcement. The research investigates shear resistance of steel fibres testing one I beam and 6 TT members. The fibre amount was 50 kg/m^3: this content can still be regarded as competitive and guarantees appreciable residual stress in uniaxial tension. Three design solutions were compared: welded wire fabric, steel fibres and plain concrete. Changing the position of the simple support, the contribution of the member-ends reinforced by steel stirrups was estimated. Fibres increase the cracking shear load and assure a quite ductile behaviour to shear collapse, although they are not as effective as stirrups are. Some equations proposed in the literature are used to predict the experimental results. A F.E. modelling is also attempted to reproduce the tests in a reduced-scale.

1 INTRODUCTION

As Batson et al. wrote almost thirty years ago (1972) the replacement of the shear reinforcement (stirrups or bent-up flexural steel) with steel fibres has some advantages. Fibres can in fact be randomly distributed trough the concrete mass at a much closer spacing than the smallest stirrups. The presence of fibres is also likely to increase the resistance to the formation and growth of cracks. The former effect is due to the crack arrest mechanism played by the closely spaced wires (Romualdi and Batson, 1963). The latter effect can be attributed to the additional energy required to pull out from concrete fibres, if not broken during the crack propagation, and to the increase in shear friction strength produced by fibres themselves. Several experimental works have been, over the past twenty years, dedicated to this interesting and promising topic, also in view of the high economical valence it has for pre-cast industry, whose features of automation and quality control make the benefits due to steel fibre addition to be fully exploited. Narayanan and Darwish (1987) in their extensive report reported results from an extensive test program on 49 beams (without any reinforcement, with traditional shear reinforcement and with fibres as shear reinforcement). Such results allowed the authors to clearly point out all the main aspects of the shear behaviour of SFRC beams, as well as to compare their performance with the ones of plain and traditionally reinforced concrete beams. It was recognised as the addition of fibres allows a transition of the failure mechanism from pure shear (brittle) to flexure (ductile); similar results have been obtained for pre-stressed pre-tensioned FRC beams.

The addition of fibres makes the failure even less catastrophic than in beams without shear reinforcement occurs, even if only fibre percentages higher than a minimum volume (1% according to Narayanan & Darwish, 1987) are able to provide the structure a significant ductility. SFRC beams also exhibited a larger first-cracking strength, not only with respect to unreinforced beams, but also to beams with stirrups. Such an improvement of the shear strength was observed to be far more significant for smaller shear spans than for larger ones, leading to hypothesise also a strengthening of the arching action of the beam due to fibres. The presence of fibres was also observed to improve the effectiveness of dowel resistance by enhancing the tensile behaviour of concrete in the splitting planes along the longitudinal flexural reinforcing bars (di Prisco et al., 1994). On the basis of a test program on SFRC large-scale girder beams, Casanova et al. (1997) concluded that steel fibres could replace traditional web reinforcement. The discontinuities in the displacement field along the crack profile were measured. A limit threshold to the crack opening displacement depending on the beam size was introduced to evaluate the shear

contribution as an average tensile residual stress acting on the crack surface. The present investigation concerns with high strength concrete pre-stressed members characterised by a thin web and a low transversal reinforcement ratio. The final aim of the experimental programme is to check the effectiveness of steel fibres when used to replace the traditional reinforcement.

2. EXPERIMENTAL PROGRAMME

Six pre-stressed TT roof elements, 7.8 m long, and one pre-stressed I beam, 7.3 m long, were tested.
The main information about the whole experimental programme is summarised in Table 1, while the geometry details of the tested prototypes are shown in Figure 1. Three different types of TT elements were chosen for the tests, all featured by the presence of a traditional web reinforcement in the heads:

- reinforced concrete elements (RC), where a uniform web reinforcement was placed along the span, according to the quantities coming out from U.L.S. design calculations;
- plain concrete elements (PC) with no web reinforcement along the length, except, as above said, for the stirrups in the heads;
- fibre-reinforced concrete elements (FRC), as before, but adding to the cast 50 kg/m^3 of steel low carbon fibers

In order to check the influence of the web reinforcement, always placed in the head of the elements for technological reasons, each type of element was tested according two different support arrangements (Figures 2 a–b). In type 1 arrangement the head reinforcement was kept inside the shear span (λ = a/d = 3.58), while it was left outside in type 2 arrangements (λ = a/d = 3.0). The I-beam was hence loaded as shown in Figure 2c, according to the classical four-point bending scheme (λ = a/d = 3.4).

Load was applied by means of a single jack (1000 kN capacity) through the device sketched in

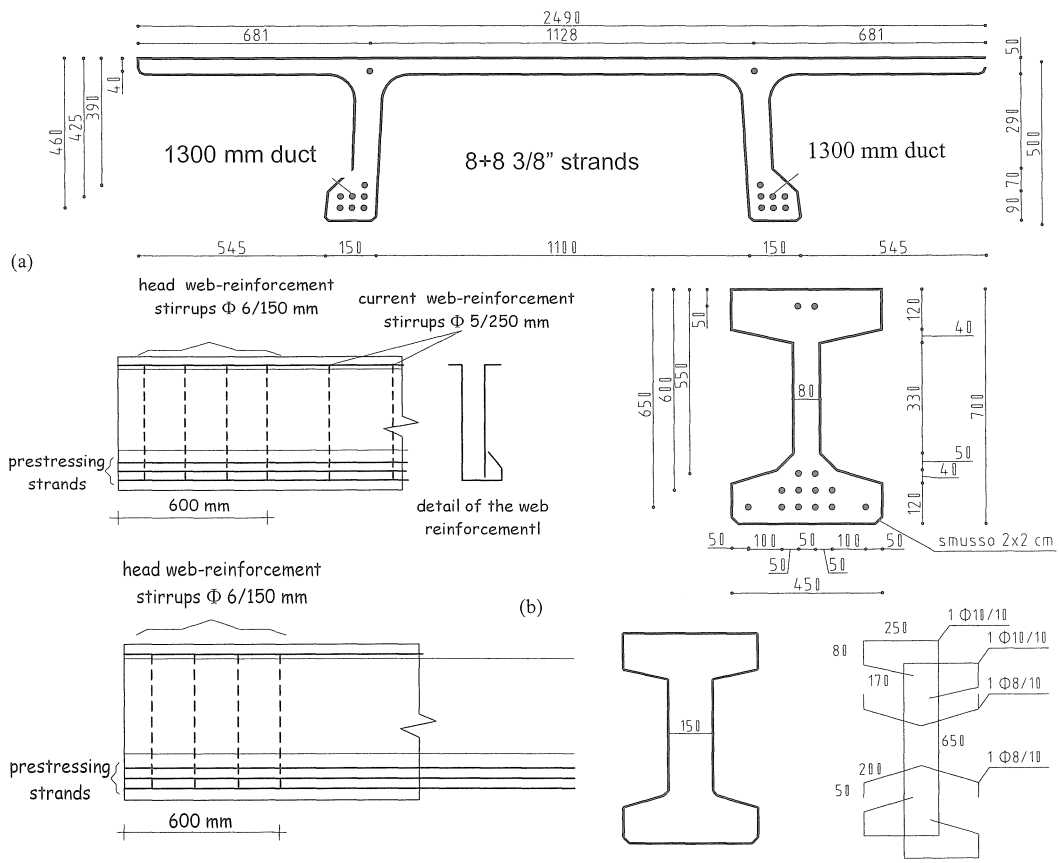

Figure 1. Geometry and reinforcement details of the tested prototypes: (a) TT element cross section, (b) TT element head reinforcement details, (c) I beams cross section and head reinforcement details.

test	Type	age [gg]	f_{ccm} [MPa]	c_f [kg/m^3]	P_{cr} [kN]	P_{max} [kN]
A1	TT50 FRC	48	86.3	50	424	540
A2	TT50 FRC	53	86.3	50	495	484
B1	TT50 PC	28	70.3	0	350	390
B2	TT50 PC	31	70.3	0	320	382
C1	TT50 RC	41	66.1	0	297	534
C2	TT50 RC	50	66.1	0	404	528
D	I-SZ70	71	81.4	50	235	283

Table 1. Test data resume.

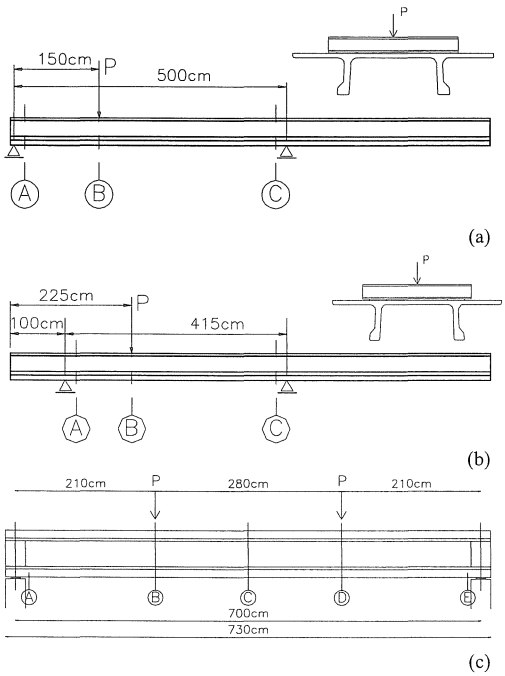

Figure 2. Loading set-up for TT elements: type 1 (a) and type 2 (b) and for the I beam (c).

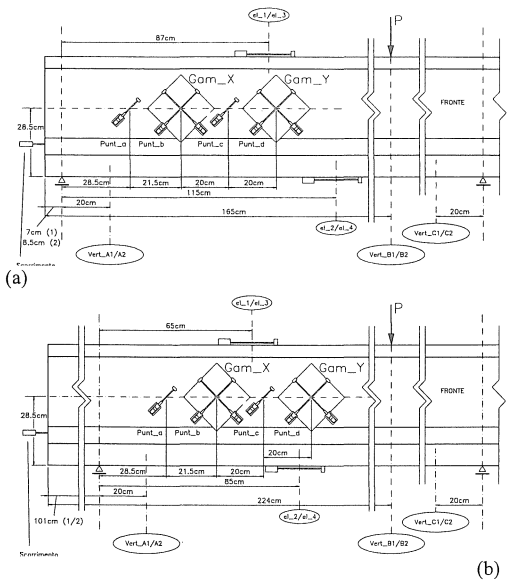

Figure 3. Positioning of the measuring instrument on the TT roof elements – test type 1 (a) and test type 2 (b)

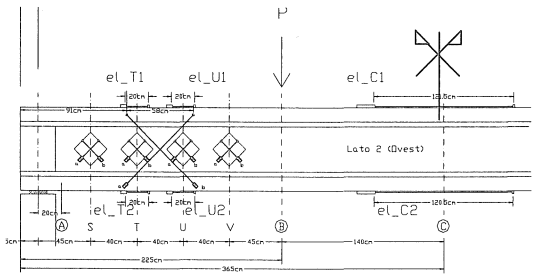

Figure 4. Positioning of measuring instruments on the I beam

Figure 2. The load steps were applied controlling the hydraulic pressure: each pressure increment was measured by a potentiometric gauge, suitably introduced in the pressure regulator, and recorded.

Besides the deflections at different locations of the cross section under the applied load and close to the supports (Vertical displacements; Figure 3), shear and longitudinal strains (γ,ε) were measured at different positions along the shear span both for the TT elements and for the beam (Figures 3,4). The gauge length was 200 mm; further compressive strains in the web (gauge length 100 mm) according to a 45° direction with respect to the longitudinal axis (with the exception in C1 test: 24° for gauge c) were also measured. All the displacements were measured by means of potentiometric gauges with a different full scale: 0-10mm for strains and 0-150 mm for vertical displacements.

3. TEST RESULTS

The global structural response, presented in terms of total load vs. load-point vertical displacement (Fig.5), shows a symmetrical deformation in the TT element webs with the only exceptions of type 2 tests for FRC element at collapse and PC element close to collapse. The failure was always reached in shear except for type 1 RC element that failed in bending. A better and more interesting comparison can be carried out by observing V-γ curves, plotted in Figure 6, grouped by test type, and in Figure 7, grouped by element type. The strain γ represents the average strain measured on the side where collapse took place.

Although the compressive strength of FRC element is the highest, an increase of the limit of proportionality is produced by fibre addition: an esti-

mation can be attempted by comparing the experimental values with the predictable ones (+24%). Steel fibres also affect the load bearing capacity: keeping the PC element as the reference, type 2 tests emphasise a quite constant fibre contribution up to a strain of 10^{-2} and can be compared to that offered by traditional reinforcement. On the contrary, type I tests are less clear. After cracking, RC and PC elements show the same stiffness. The slight increase in the load observed is probably due to the activation of an arch mechanism built on the head reinforcement, as explained further. The reduced ductility of RC element reveals the collapse in bending.

The head-reinforcement influence can be appreciated comparing the curves for the same element (FRC, RC or PC) tested in both the load arrangements (type 1 and type 2 tests; see Figure 7 a,b,c). For PC structures, the load bearing capacity at failure is practically independent on the load arrangement, but the path followed by type 1 test is stiffer. By contrast, FRC type 1 test follows the less stiff path and increases the shear load bearing capacity for high strain values. To conclude, the head-reinforcement favours the formation of an arch-mechanism that improves the ductility of the structure at failure and partially its load bearing capacity when the structure is transversally reinforced.

The analysis of the compressive strains in the TT top chords highlights a sudden snap at the onset of the collapse. It corresponds to the bending of the compressed chord that contributes to the total shear-load capacity. The compressive strains measured in the TT-webs, tested in type I load arrangement, highlight the role of the reinforcement. A quite uniform diagonal compression field develops in the FRC element and the RC element exhibits a progressive growth in the participation of the strut closer to the load-point. On the contrary, in the PC element the most active strut is the nearest to the support region.

The crack patterns at collapse confirm the previous observations. In particular, in type-2 load arrangement, only one crack propagates in FRC and PC elements whereas the RC structure shows two cracks in the web with a similar inclination.

The behaviour of the pre-stressed I-beam differs from the other structures essentially for the cracking induced by the sliding action between the web and the compressed chord (Figure 11). This post-cracking resistant mechanism is characterised by hardening as push-off test can prove (Khaloo, A.R. & Kim, 1997). A fan-shape strut originates up to the opening of an inclined crack that causes the structural failure. The increase of the shear strain read for the S gauge location (Figure 10) is justified by the progressive sliding of the first crack formed close to the beam-end.

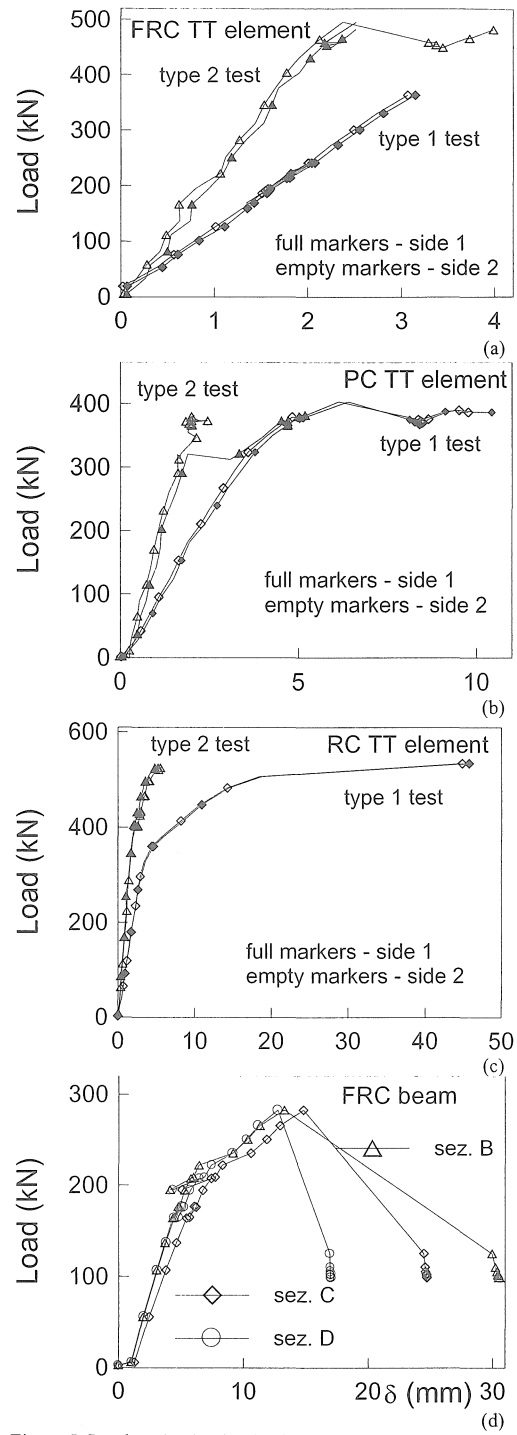

Figure 5. Load vs. load point displacement curves

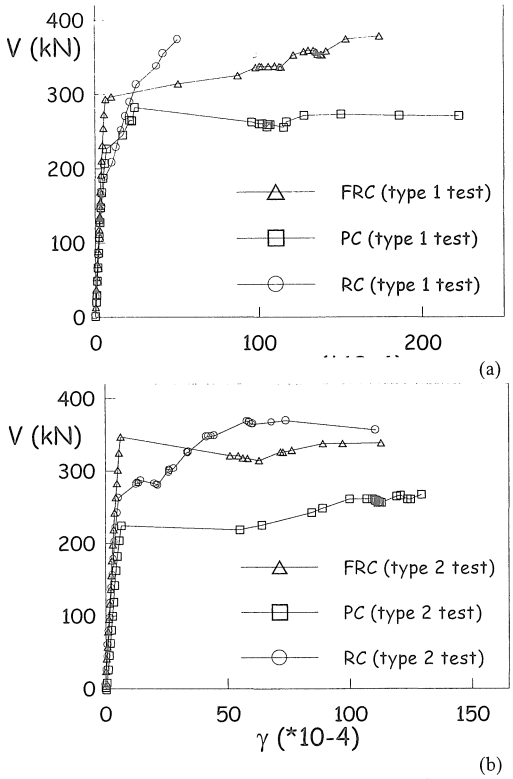

Figure 6. V-γ curves for type 1(a) 2(b) tests on TT elements.

4. DISCUSSION OF TEST RESULTS

Various shear resistant mechanisms develop within the structures at issue and can interact at collapse. A first attempt to interpret the test results has been performed through formulae suggested by standard codes as well as available in the current literature (di Prisco & Romero, 1996).

A rough evaluation is summarised in Table III (See Appendix I). The ratio between the expected shear-load capacity and the experimental one has been plotted for each test (Figure 12). Except for the Nielsen & Braestrup's model, that roughly overestimates the shear capacity, the other formulae are likely to account only for a limited fraction of the shear load carried by the structures. Therefore, the superposition of the arch mechanism (Table III; d) with a mechanism that computes all the web mechanisms (Table III; a, b or c) seems predict quite well the experimental values. It is worth to note that the superposition cannot compute both the mechanisms with their maximum load bearing capacity. The crack patterns at failure (Figure 11) reveal one dominant crack. Such a crack isolates an almost integer portion of the element close to the support, where an arch mechanism is likely to

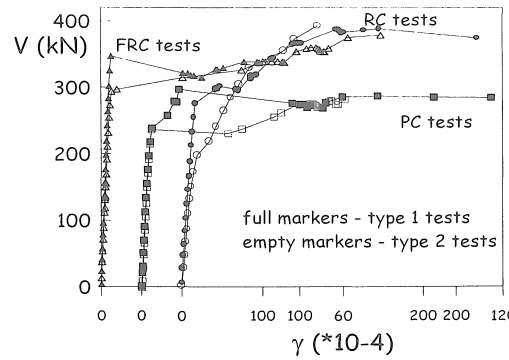

Figure 7. V-γ curves for FRC, PC and RC elements.

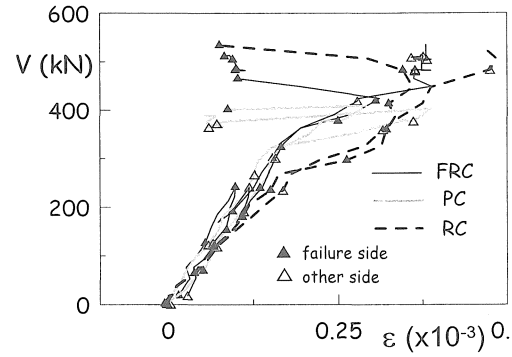

Figure 8. Compressive strains in top chords (type 1 test)

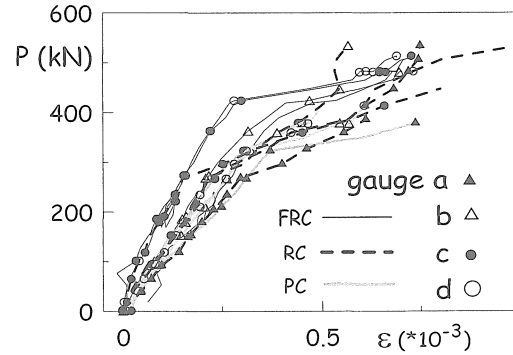

Figure 9. Compressive strains in the web (failure side-type 1 test)

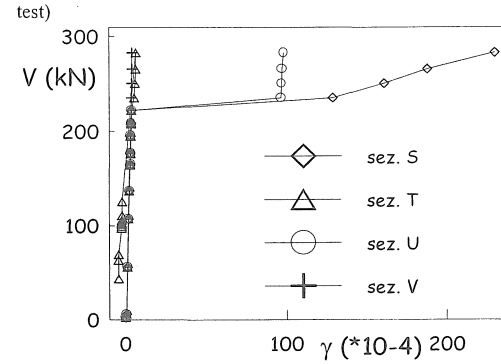

Figure 10: V - γ curves for the I beam

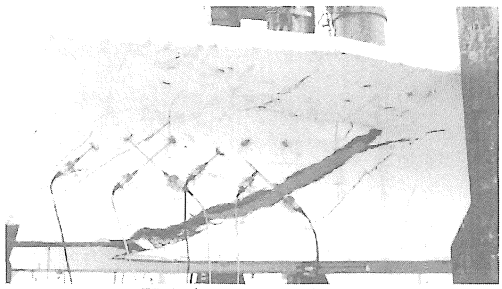

FRC element – type 1 test

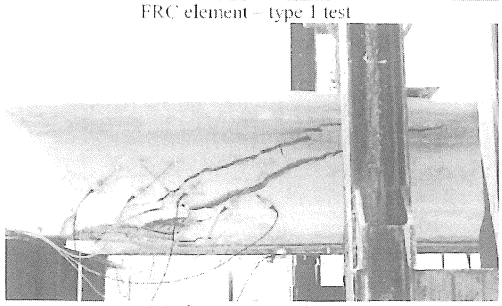

PC element – type 1 test

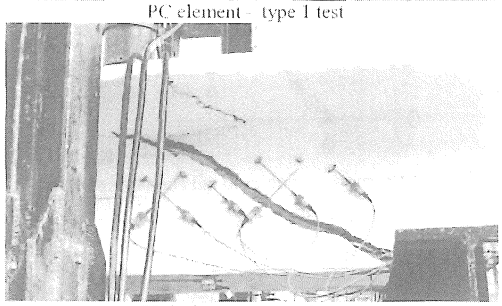

FRC element – type 2 test

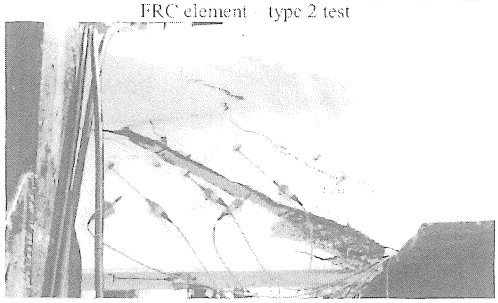

RC element – type 2 test

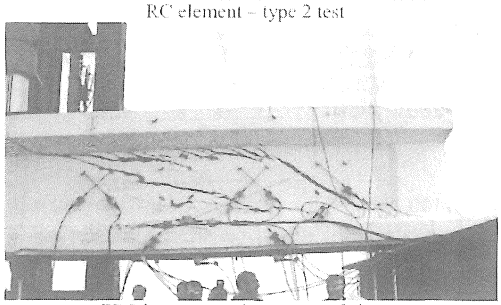

FRC beam – crack pattern at failure

Figure 11. Crack patterns at failure

develop, carrying a significant part of the total shear, besides the classical truss or comb mechanism. A further contribution may come from a "fan-arch" mechanism that develops, besides the classical one, taking from the flexural deformation of the upper plate of the TT element. The increase in the shear load capacity offered by the reinforcement is emphasised, for type 2 tests, in Figure 13.The contribution is traced as a function of a component of the crack opening displacement detected by a 45° oriented gauge positioned along the dominant crack. It is worth to note that the passive confinement exerted by fibre pull-out less favourably interact with aggregate interlock than stirrups, but seems to be more efficient in arresting the crack propagation.

A confirmation of all the above exposed hypotheses has been searched with the aid of finite element analysis, both in the linear-elastic and non-linear field. Linear elastic analyses were performed on a true scale 3D model, taking for the element cross section. 6(8)-node prism elements were used for the web(wing)-concrete, while the cables were modelled by means of bar elements, connected to the concrete nodes. Pre-stressing was assigned through an equivalent thermal strain of the bar elements.

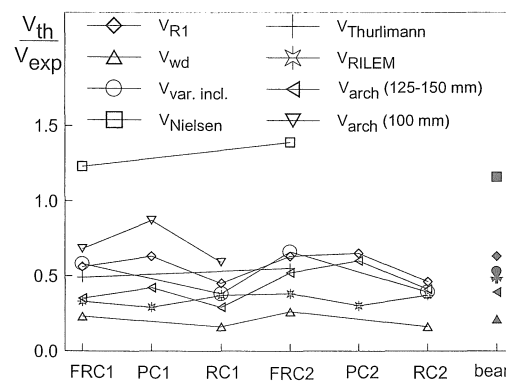

Figure 12. Theoretical/experimental shear ratios

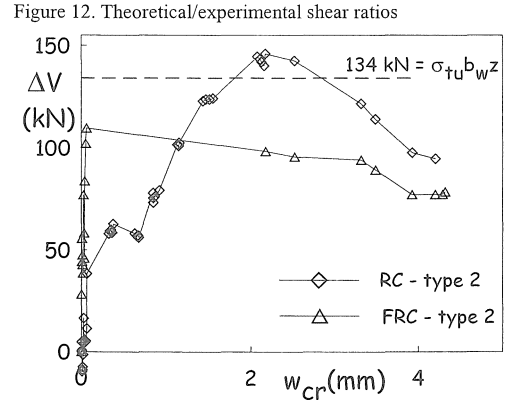

Figure 13. Reinforcement shear load capacity (type 2 tests)

In Figure 14 the mesh employed for such analysis is shown. Concrete was assigned E_c = 40 GPa and ν = 0.2; for pre-stressing steel E_s = 200 GPa ,ν = 0.3 and f_{sy} = 1900. MPa were chosen.

Besides the elastic 3D analysis a 2D non-linear analysis was performed. The TT element was actually modelled as a panel, concrete in the upper and bottom chord having been assigned a fictitiously amplified stiffness to take for the different thickness of the slab and of the bulbs respectively. Only concrete in the web inside the supports was treated by means of the crush-crack non-local damage model (di Prisco and Mazars, 1996; Ferrara and di Prisco, 2000); material in the web outside the supports as well as everywhere in the lower and upper chords was left simply linear elastic. Such a choice has to be motivated surely by reasons of computational convenience but also in order to prevent some spurious flexural damage detected in the lower bulb, if modelled as a damageable material. Furthermore, in order to fully exploit the benefits of non-local regularisation, and still for the sake of computational charges, the 2D model was actually reduced with respect to the true scale element. The ratio between this and the former was set equal to 5, as a reasonable compromise between the geometrical size of the finite element model and the minimum element size guaranteeing the effectiveness of the non-local algorithm, for the assigned value of the characteristic length ($h = d_a = 15\ mm$). Non-linear analysis was performed only for the case of FRC element tested according to load arrangement 2. Materials properties, estimated on the basis of characterisation tests performed on a similar material, are hereafter summarised:

Table II: material properties employed in numerical analyses

f_c (MPa)	61
f_t (MPa)	4.12
σ_{res} (MPa)	1.2
G_f (N/mm)	116

A comparison between the 3D and the 2D reduced model, in the elastic field, can be done by observing, in Figure 15, normal and shear stresses at the bounds of web-field of the TT element included between the left support and the load-point. Elastic analyses on the 3D and the 2D reduced model were performed by applying a load proportionally scaled according to the adopted geometry scaling ratio. Curves in Figure 15 show a good correspondence between the full scale 3D model and the 2D reduced one. Such curves also clearly show the presence of a "discrete" arch shear resistant mechanism, between the left support and the load-point. The fan-shaped arch, "smeared" all over the web panel in the shear span, is likely to play a less relevant contribution, as the almost constant trend of both shear and normal stresses at the panel-upper slab boundary is likely to confirm.

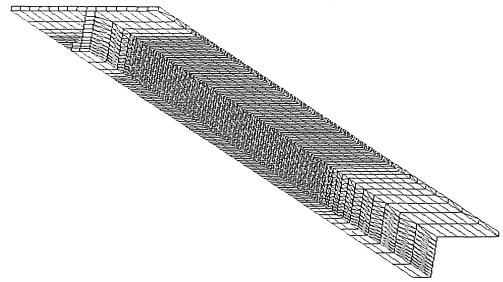

Figure 14. Mesh employed for 3D analysis of the TT element

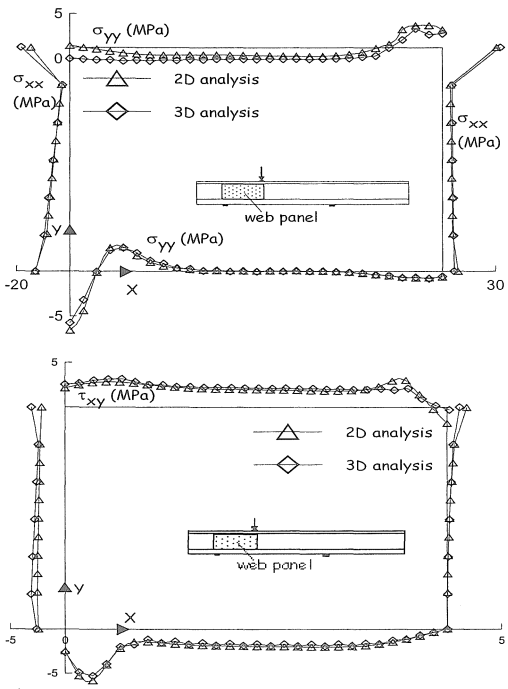

Figure 15. Stresses at the bounds of the web panel

The damage pattern at the computed maximum load (Figure 15) clearly shows, within an almost uniformly damaged field, a diagonal crack, whose trend is likely to resemble the experimentally detected one (Figure 11). The numerical analysis having been performed under load control and with linear elastic material in the lower bulb, it was not possible to follow the unstable branch after the maximum load. In such a stage the complete crack propagation up to the load point and downward, towards the left support though the lower bulb, was observed. Load-displacement curves, compared in Figure 16, show a quite good agreement between experiments and numerical predictions. As far as the 2D numerical curve is concerned, having the analysis been performed on a reduced-scale model, the size effect has also to be considered. To the authors' knowledge no reference could be found in the literature applying to the case at issue. A rough

evaluation of the nominal shear strength, computed as $\tau_u = V_{max}/bz$, with z internal lever arm, yielded the following values:

τ_u = 12.2 MPa (numerical)

τ_u = 5.4 MPa (experimental).

the ratio being roughly equal to $\sqrt{5}$, close to the predictions of a classical LEFM size-effect law.

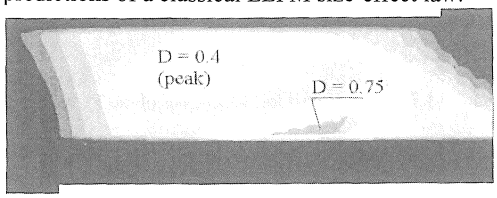

Figure 15.Damage at peak load (2D non-local analysis)

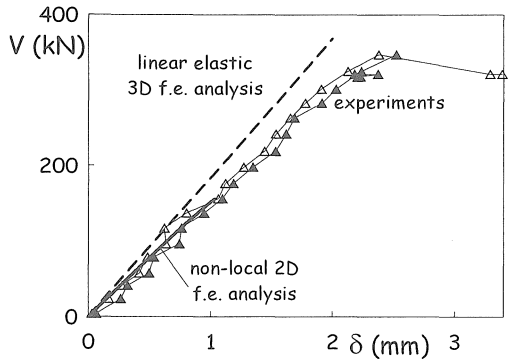

Figure 16. Numerical/experimental load-displacement curves

5 CONCLUDING REMARKS

- Shear capacity of TT elements can be reliably predict by means of code formulae, considering, besides web mechanisms, the bearing capacity of a parallel-acting arch mechanism. Traditional web reinforcement makes the shear capacity to increase, also due to a positive interaction with aggregate interlock.
- Fibre contribution can be estimated through equations proposed by Casanova et al.; an evaluation of the residual tensile stress has to be performed, in a reliable crack-opening range.
- Fibre reinforcement can be designed as alternative to stirrups for weak reinforcement ratios on the basis of the following equation:

$$\sigma_{tu} = \alpha V_f \frac{l_f}{d_f} \tau_u = k \rho_t f_{sy},$$

set k ≅ 0.8 a sort of efficiency factor. Further experiments need to check the dependence of k on the fiber volume fraction.

- Non-local damage analysis on scaled models can be a valuable help for the interpretation of experiments, provided that results were calibrated on a reliable size effect law.

ACKNOWLEDGEMENTS

The authors thank LARCO-ASTORI for the financial support and M.Sc. C. Failla, Dr. R. Felicetti and Prof. G. Toniolo for the precious cooperation in the experimental investigation

REFERENCES

Batson, G., Jenkins, E., Spatney, R., 1972. Steel fibers as shear reinforcement in beams, *ACI Journal*, 69: 640-644.

Casanova, P., Rossi, P., Schaller, I., 1997. Can steel fibers replace transverse reinforcements in reinforced concrete beams?, *ACI Mat. J.* 94, 5: 341-354.

di Prisco, M., Caruso, M.L., Piatti, S., 1994. On fiber role in dowel action, *Studi e Ricerche*, 15:151-194. School of Specialisation on R/C Structures, Politecnico di Milano.

di Prisco, M. & Mazars, J. 1996. Crush-Crack: a Non-local Damage Model for Concrete, *Mechanics of Cohesive-Frictional Materials and Structures*, 1: 321-347.

di Prisco, M. & Romero, J., 1996. Diagonal Shear in Thin-Webbed Reinforced-Concrete Beams: Fiber and Stirrup Roles at Shear Collapse, *Mag. Concr.Res.*, 48(174): 1-18.

Ferrara, L. & di Prisco, M. (in press). Mode I fracture behavior in concrete: non-local damage modelling, *J. Engrg. Mechs, ASCE.*

Khaloo, A.R. & Kim, N., 1997. Influence of concrete and fiber characteristics on behavior of steel fiber reinforced concrete under direct shear, *ACI Mat. J.*, 94 (6): 592-601.

Narayanan, R. & Darwish, I.Y.S., 1987. Use of steel fibers as shear reinforcement, *ACI Struct. J.*, 84 (3): 216-227.

RILEM TC162-TDF. 2000. Test and Design Methods for Steel Fibre Reinforced Concrete: Recommendations. σ-ε-Design method. *Materials and Structures*, 33: 75-81.

Romualdi, J.P. & Batson, G.B.,1963. Mechanics of crack arrest in concrete, Proc. ASCE, 89 EM3: 147-168.

Table III. Formulae for the shear capacity of tested structures

APPENDIX I

a	$V = V_{R1} + V_{wd}$	
	V_{R1}	Structure with no shear reinforcement (EC2) $V_{R1} = [0.25\, f_{ctd}\, \kappa\, (1.2+40\rho_s) + 0.15\, \sigma_{cp}]\, b_w\, d$
	V_{wd}	Shear capacity of the web reinforcement $V_{wd} = 0.9\, b_w\, d\, \mathrm{cotg}\psi^I\, \omega_w\, f_{c2}$ $\omega_{wz} = a_{sw} f_{yw} / b_w f_{c2} + \alpha_f V_f \tau_f^u l_f / d_f f_{c2}$
b	$V_{in.\ var.}$	Variable inclination truss model $V_{in.\ var.} = \mathrm{ctg}\psi\, \omega_w\, b_w\, z\, f_{c2}$
	V_{Thurl}	Thurlimann model: $V_{Thurl.} = \tau_u\, b_w d$ $\frac{\tau_u}{f_{ck}} = 2(\omega_{st} + \varsigma_f)$ $\varsigma_f = \frac{\sigma_{tu}}{f_{ck}} = \alpha_f V_f \tau_f^u / f_{ck} (l_f / d_f) \eta_p$
	V_{Niels}	Nielsen - Braestrup model: $V_{Nielsen} = \tau_u\, b_w d$ $\frac{\tau_u}{f_{ck}} = \sqrt{[-\omega_{st}^2 + (\nu - 2\varsigma_f)\omega_{st} + (\varsigma_f \nu - \varsigma_f^2)]}$
c	V_{Rilem}	RILEM model
d	V_{arch}	Arch mechanism capacity: $V_{R2}^{ARCH} = 0.4 \frac{f_{c2} b_w d}{1+\lambda^2}$